RESEARCH ARTICLE



Check for updates

On the reliability of atoms in molecules, noncovalent index, and natural bond orbital to identify and quantify noncovalent bonds

Steve Scheiner



Department of Chemistry and Biochemistry, Utah State University, Logan, Utah, USA

Correspondence

Steve Scheiner, Department of Chemistry and Biochemistry, Utah State University, Logan, UT 84322-0300. USA.

Email: steve.scheiner@usu.edu

Funding information

National Science Foundation, Grant/Award

Number: 1954310

Abstract

Atoms in molecules, noncovalent index, and natural bond orbital methods are commonly invoked to identify the presence of various noncovalent bonds and to measure their strength. However, there are numerous instances in the literature where these methods provide contradictory or apparently erroneous interpretations of the bonding. The range of reliability of these methods is assessed by calculations of a variety of systems, which include an H-bond, halogen bond, π -tetrel bond, CH-HC interaction, and a pairing of two anions. While the results appear to be meaningful for the equilibrium geometries, and those where the two subunits are progressively pulled apart, these techniques erroneously predict a progressively stronger bonding interaction as the two units are compressed and the interaction becomes clearly repulsive. The methods falsely indicate a bonding interaction in the CH-HC arrangement, and incorrectly mimic the behavior of the energy when two anions approach. These approaches are also unreliable for understanding angular deformations.

KEYWORDS

antielectrostatic, $\mbox{H}{\cdot\cdot}\mbox{H}$ interaction, halogen bond, H-bond, tetrel bond

1 | INTRODUCTION

Noncovalent bonds are of course considerably weaker than their covalent counterparts, sometimes by an order of magnitude. As a variation on the venerable H-bond, $^{1-5}$ noncovalent bonds of most recent interest replace the central proton by a nominally electronegative atom such as Cl or As. The ensuing interaction is typically named after the family of the periodic table from which this atom is derived, e.g. halogen or pnicogen bond. $^{6-22}$ These prior studies have shown than an important component of the bonding arises from a depletion of electron density in a limited region surrounding this central atom, whose positive charge attracts a nucleophile. In a common situation, this density depletion occurs along the antipode of an R-X covalent σ -bond (where X refers to the central atom), and so is termed a σ -hole. However, there are also numerous instances where the positive region lies above the atom in question within a planar or linear segment, leading to its designation as a π -hole. In either case, the

Coulombic attraction is supplemented by a certain amount of charge transfer from the nucleophile/Lewis base to the appropriate antibonding orbital of the Lewis acid unit. Other components that add to the stabilization are connected with overall polarization of the two subunits and a varying amount of London dispersion attraction.

Quantum calculations are frequently invoked to probe into the origin and strength of a given noncovalent bond. As a sort of ultimate yardstick, the binding energy is straightforwardly evaluated as the drop in energy that arises when the two monomers are allowed to interact with one another. A common first step in understanding this quantity derives from elucidation of the molecular electrostatic potential (MEP) surrounding each monomer as a three-dimensional image. The magnitude and depth of any σ or π -hole can then be explored as one important element of the associated electrostatic interaction with the nucleophile. The charge transfer between the two units is usually dominated by the aforementioned transfer from nucleophile lone pair to the σ^* or π^* antibonding orbital of the Lewis acid, a quantity which

Natural Bond Orbital (NBO) formalism is well designed to measure. The interaction between the two subunits perturbs the total electron density, and bonding interactions can be visualized via the identification of intermolecular bond paths via Atoms in Molecules (AIM) analysis of the topology of the density. Certain quantities can be evaluated at the bond critical point (BCP), whose magnitudes are commonly taken as a quantitative measure of the strength of that bond. A related means of quantifying any bonding interactions comes from the Noncovalent Index (NCI) procedure where minima in a reduced density gradient (RDG) are presumed to help identify bonding interactions, and to distinguish them from destabilizing repulsive forces.

There are numerous instances in the literature in which NBO, AIM, and NCI have been applied where the various methods agree with one another and with the overall energetics. Indeed, quantitative relationships have been derived in certain classes of systems and usefully applied where the binding energy can be simply related to one or more indicators derived from these methods. For example, it is common in the literature to consider the bond critical point density as a measure of bond strength^{23–27} and possibly even with spectroscopic perturbations.²⁸ In an alternate scheme, the energies of some of these bonds are sometimes assessed via a simple relationship with the potential energy density^{24,29–31} or other quantities extracted from AIM analysis.^{24,27,32–34}

It would indeed be comforting for analysis of noncovalent bonds if the methods indicated above provided definitive indicators of the presence of such a bond, and if the data could be treated in a quantitative manner to compare strengths of such bonds. However, there have been numerous examples where the various methods conflict with one another as to which sorts of bonds might be present. 35-38 There have also been numerous cases described in the literature where AIM locates a bond path where no such bond would appear to exist, or worse, that the interaction in question is a repulsive one. 36,39-44 Another sort of dismaying occurrence is the failure of AIM to identify a bond that is actually present. 45

The present work constitutes an attempt to more thoroughly address these issues and to differentiate situations where some or all of these metrics represent a reliable indicator of the presence of a bond from those where they provide spurious or misleading clues. A wide range of different sorts of interactions are considered here so as to broaden the utility of the findings. The classical H-bond in the CIH.·NH₃ dimer is considered first, followed by a typical halogen bond in FBr··NH₃. A π -hole tetrel bond is included via the placement of the NH₃ nucleophile above the molecular plane of H₂CO. In order to address the controversy in the literature 40,42,46-50 as to whether a bond path between two H atoms signifies a stabilizing force, a pair of CH₄ molecules are aligned in a CH··HC configuration. There has been a recent flurry of activity⁵¹⁻⁶⁰ dealing with the question as to whether a pair of ions of like charge can attract one another under certain circumstances, an issue which is addressed here by pairing the CN⁻ and MgCl₃⁻ anions.

In each of these systems, the various noncovalent bond indicators are monitored as the two units are brought closer and closer together, whereby the interaction becomes progressively stronger and then turns repulsive. Rather than focusing solely on the distance between the two subunits, calculations were also performed in order to examine the effects of angular deformations, which are well known to weaken these noncovalent bonds and even lead to their disappearance. The central question in all of these systems concerns the ability of NBO, AIM, and NCI to serve as reliable measures of the presence and strength of a bond. Importantly, all of the systems are chosen so that the particular interaction of interest is the only one present, thereby avoiding complications that would arise in the interpretation if additional bonding were present.

2 | METHODS

Quantum chemical calculations were carried out with the aid of the Gaussian 16⁶¹ suite of programs. Density functional theory (DFT), with the M06-2X functional, 62 was used in conjunction with the augcc-pVTZ basis set⁶³ adding both polarization and diffuse functions onto a triple-ζ foundation. The accuracy of this approach has been affirmed by numerous past calculations of related systems.⁶⁴⁻⁶⁹ The binding energy E_b is defined as the difference between the energy of the dimer and the sum of the energies of the two monomers in their optimized geometry. This quantity was evaluated for the equilibrium structure of each dimer, as well as geometries including stretching and bending deformations. The AIM method identified bond paths, and the properties of their bond critical points, in the context of the AIMAII⁷⁰ program. The Noncovalent Index procedure was implemented via the Multiwfn program⁷¹ which provided quantitative measures of the reduced density gradient, and was illustrated graphically in molecular space by VMD.⁷² Individual orbitals, and the energetic contributions of charge transfers between them, were assessed by Natural Bond Orbital (NBO) theory 73,74 via the NBO program incorporated into Gaussian. Total interaction energies were decomposed into physically meaningful components by the Symmetry-Adapted Perturbation Theory (SAPT) protocol^{75,76} with the aid of the MOLPRO program,⁷⁷ within the context of the aug-cc-pVTZ basis set.

3 | RESULTS

3.1 | Distance dependence

3.1.1 | H-bond

The complex between HCl and NH_3 represents a classic H-bond motif, illustrated in Figure 1A. According to the data in Table 1, as the two units approach one another, starting from $R(H \cdot N) = 2.5$ Å, the energy continues to decline as the geometry reaches its optimum separation of 1.69 Å and with a binding energy of -8.97 kcal/mol. During this approach, the various markers of the H-bond strength increase in magnitude. In particular, the electron density at the bond critical point climbs to 0.0596 au. The Laplacian of the density at the same point is positive which indicates a noncovalent bond, and is equal to

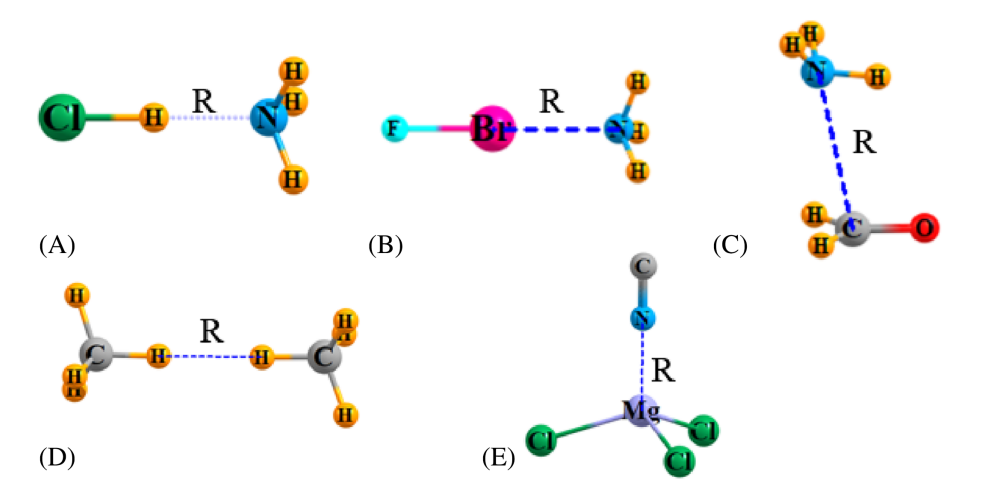


FIGURE 1 Molecular diagrams of systems studied

R(H.·N) (Å)	E _b (kcal/mol)	ho (au)	$ abla^2 ho$ (au)	− V (au)	E(2) (kcal/mol)	sign(λ_2) ρ (au)
2.5	-4.29	0.0099	0.0278	0.0046	4.1	-0.0101
2.1	-6.90	0.0233	0.0552	0.0148	13.8	-0.0240
1.9	-8.20	0.0372	0.0565	0.0283	25.5	-0.0420
1.69	-8.97	0.0596	0.0461	0.0537	46.4	-0.0499
1.5	-7.76	0.0908	0.0298	0.0925	80.5	-
1.3	-1.82	0.1471	-0.1019	0.1823	148.5	-
1.1	+15.79	0.2476	-0.8190	0.4421	292.6	-

TABLE 1 Behavior of various properties as CIH and NH₃ approach one another in H-bond

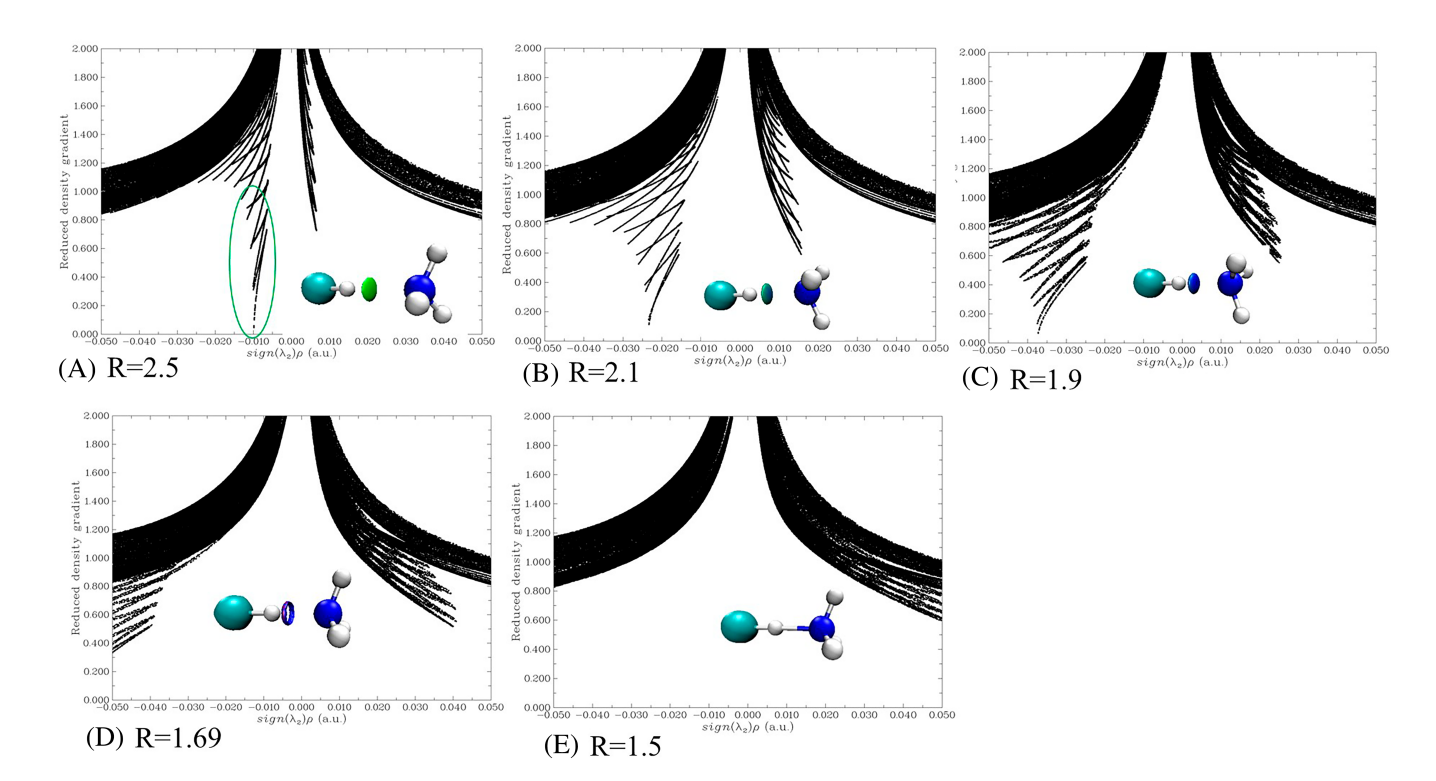


FIGURE 2 Noncovalent index diagrams of CIH··NH₃ complex for various values of $R(H \cdot N)$ (Å). Extrema of sign(λ_2) ρ are shown in blue for -0.035 au and red for +0.020 au

TABLE 2 Behavior of various properties as FBr and NH_3 approach one another in σ -hole halogen bond

R(Br··N) (Å)	E _b (kcal/mol)	ho (au)	$ abla^2 ho$ (au)	−V (au)	E(2), kcal/mol	sign(λ_2) ρ (au)
2.9	-9.99	0.0178	0.0564	0.0113	10.0	-0.0189
2.6	-13.18	0.0335	0.0906	0.0255	22.6	-0.0375
2.35	-14.70	0.0583	0.1108	0.0527	47.1	-0.0500
2.1	-11.15	0.0951	0.1216	0.1088	88.0	-
1.9	+2.27	0.1401	0.1405	0.2103	144.8	-
1.7	+37.68	0.2066	0.3646	0.4422	-	-

0.0461 au at the equilibrium point. The potential energy density V becomes increasingly negative, signaling a strengthening bond. V is equal to -0.0537 au at the equilibrium, corresponding to 33.7 kcal/mol. Half of this amount is sometimes taken as a measure of the H-bond strength, 29 but 16.8 kcal/mol is quite a bit larger than the actual E_b of 9.0 kcal/mol. The NBO second-order perturbation energy E (2) corresponding to transfer from the N lone pair to the σ^* (HCI) antibonding orbital reaches 46.4 kcal/mol at the equilibrium structure. With regard to NCI analysis, values listed in the last column of Table 1 represent the most negative value of $sign(\lambda_2)\rho$ in the vicinity of the H-bond, which reaches -0.0499 au at the equilibrium contact distance.

Importantly, as the two units are compressed together to contact distances shorter than their equilibrium separation, and the energy of the system begins to climb, the noncovalent bond strength markers continue along on the same pattern of signaling a stronger bond. The BCP density rise dramatically, reaching 0.2476 au, even when the interaction has turned repulsive by 16 kcal/mol. As the distance drops below 1.5 Å, $\nabla^2 \rho$ reverses sign, and even becomes very negative, indicative of a covalent bond. V also continues to increase in magnitude, as does $\it E(2)$ which rises to nearly 300 kcal/mol.

The NCI analysis, however, no longer contains an indication of a H··N bonding interaction for R shorter than the equilibrium separation. The evolution of the NCI analysis can be visualized in Figure 2 which plots the reduced density gradient vs $\operatorname{sign}(\lambda_2)\rho$. As the two monomers approach one can see that the tendrils enclosed by the green oval in Figure 2A, which corresponds to the green disk in the insert diagram, shifts to the left, i.e. to more negative values of sign $(\lambda_2)\rho$. This displacement is quantified by the values tabulated in Table 1, indicative of the strengthening bond. The colored disk in the insert changes color from green to blue which corresponds also to a more negative $\operatorname{sign}(\lambda_2)\rho$. These tendrils disappear in Figure 2E when the two molecules are pulled in to repulsive contact distance.

3.1.2 | Halogen bond

The approach of NH $_3$ to the Br atom of FBr along the F-Br axis constructs a typical σ -hole halogen bond involving electron donation from the N lone pair to the σ^* (FBr) orbital, as represented in Figure 1B. The equilibrium R(BrN) distance is 2.35 Å, with a halogen bond energy of -14.7 kcal/mol, as displayed in Table 2. Consistent with the H-bond trends, ρ , $\nabla^2 \rho$, V, and E(2) all rise in magnitude as the two molecules come closer, and continue to do so even after they have passed the

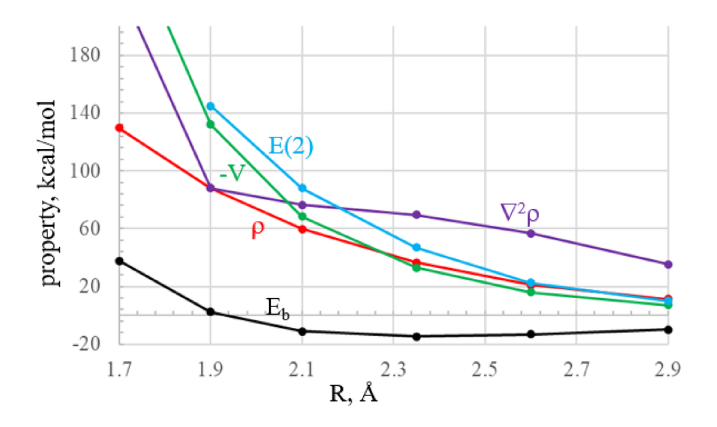


FIGURE 3 Dependence of various properties on $R(Br \cdot N)$ for FBr··NH₃ complex. ρ and $\nabla^2 \rho$ are multiplied by 627.5 kcal/mol/au

equilibrium distance and the interaction has turned repulsive. There is a minor difference in that $\nabla^2 \rho$ does not turn negative for the halogen bond and that E(2) cannot be evaluated for R=1.7 Å since NBO treats the system as a single unit, but otherwise the trends remain intact. The same can be said for the NCI data where $\operatorname{sign}(\lambda_2)\rho$ becomes progressively more negative until vanishing for distances closer than equilibrium. The NCI diagrams for this system are quite similar to Figure 2, and are presented in Figure S1.

The manner in which each element varies as the two molecules are drawn in toward one another is shown graphically in Figure 3. For purposes of comparison, all quantities are expressed in kcal/mol in the figure. There is a clear contrast between the energy (the black curve) which bottoms out at R=2.35 Å, and the AIM and NBO indicators of bond strength all of which climb monotonically as R decreases, even well past the minimum in the energy.

3.1.3 | π -Hole tetrel bond

In addition to interacting with the positively charged $\sigma\text{-hole}$ of, for example a halogen atom, a number of molecules contain a positive region above their molecular plane, commonly referred to as a $\pi\text{-hole}$. The H_2CO molecule is an example, where such a $\pi\text{-hole}$ lies above the C atom, which can interact with a nucleophile such as NH $_3$ to form a $\pi\text{-hole}$ tetrel bond. This sort of arrangement is pictured in Figure 1C where the optimal positioning of the NH $_3$ is 2.81 Å above the C. The binding energy of the two subunits is -3.97 kcal/mol, as indicated in the first row of Table 3. In this

R(C.·N) (Å)	E _b (kcal/mol)	ho (au)	$ abla^2 ho$ (au)	−V (au)	E(2) (kcal/mol)	$\operatorname{sign}(\lambda_2) \rho$ (au)
2.81	-3.97	0.0128	0.0457	0.0081	4.3	-0.0135
2.6	-3.68	0.0185	0.0671	0.0135	7.3	-0.0197
2.4	-1.99	0.0280	0.0966	0.0228	14.0	-0.0311
2.2	+1.99	0.0444	0.1235	0.0393	28.8	-0.0500
2.0	+9.07	0.0707	0.1338	0.0693	58.7	-0.0500

TABLE 3 Behavior of various properties as H_2CO and NH_3 approach one another via π -hole tetrel bond

R(H.·H) (Å)	E _b (kcal/mol)	ho (au)	$ abla^2 ho$ (au)	−V (au)	E(2) (kcal/mol)	sign(λ_2) ρ (au)
3.5	-0.09	0.0004	0.0014	0.0001	-	-0.0004
3.0	-0.11	0.0010	0.0040	0.0004	-	-0.0011
2.6	-0.04	0.0025	0.0087	0.0011	0.1	-0.0026
2.2	+0.23	0.0061	0.0189	0.0030	0.3	-0.0062
2.0	+0.61	0.0094	0.0289	0.0052	0.6	-0.0095
1.8	+1.42	0.0146	0.0443	0.0093	1.1	-0.0152
1.6	+3.09	0.0229	0.0635	0.0172	2.4	-0.0236
1.4	+6.42	0.0370	0.0730	0.0326	5.5	-0.0397
1.2	+12.85	0.0602	0.0541	0.0624	12.0	-0.0500

TABLE 4 Behavior of various properties as two CH₄ molecules approach one another in CH··HC arrangement

optimized configuration, the density at the bond critical point is 0.0128 au, with a positive density Laplacian, consistent with a non-covalent bond. There is an appreciable transfer of charge from the N lone pair to the $\pi^*(CO)$ orbital, with E(2)=4.3 kcal/mol, and sign $(\lambda_2)\rho$ is equal to -0.0135 au, symptomatic of a moderately strong noncovalent bond.

For each new $R(C \cdot N)$ distance, the remainder of the geometry was fully optimized. As the two monomers are compressed toward one another, the potential is repulsive, and E_b quickly reduces in magnitude and then turns positive. However, all of the bond indicators suggest a progressively stronger bond: ρ , $\nabla^2 \rho$, V, and E(2) all rise in magnitude, as does the NCI measure in the last column of Table 3. Even when the bond length has been shortened to 2.0 Å, a full 0.8 Å shorter than the optimized value, and E_b has changed from -3.97 to +9.07 kcal/mol, these various metrics are large and still growing. The effects of the bond contraction upon the NCI diagrams are shown explicitly in Figure S2 where the insets depict the morph of the central bonding region from green to blue, indicative of growing bond strength.

3.1.4 | Direct H.·H interactions

Several quantum studies in the literature have noted AIM bond paths between H atoms on different molecules which have led to a discussion concerning the possibility of H··H bonds. $^{40,42,46-50}$ These suggestions of a H··H bond are puzzling in that the two H atoms have similar overall charge, unlike the situation in dihydrogen bonds where the two atoms have opposite charge, and such attractions can be explained on electrostatic grounds. In an effort to unravel the nature of these purported bonds, a pair of CH₄ molecules were arranged so as to contain a linear CH··HC axis, as depicted in Figure 1d. The

distance between the two monomers was diminished in small decrements, beginning from $R(H \cdot \cdot H) = 3.5$ Å. As is evident in Table 4, there is a very shallow minimum of 0.1 kcal/mol that occurs at about R = 3.0 Å, but this attraction quickly morphs into a repulsion with positive E_b as the two units are drawn in further toward one another, becoming especially repulsive for R less than about 1.6 Å.

As this is a very weak interaction, it is not surprising that the bond strength metrics are quite small for large R. In fact, NBO does not indicate any charge transfer from the $\sigma(CH)$ bonding orbital of one monomer to the $\sigma^*(CH)$ antibond of the other (and vice versa) until R is 2.6 Å or less. However, most importantly, despite the repulsive nature of the potential, all measures indicate the presence of a H··H noncovalent bond, and these metrics all agree that the bond grows in strength as the two units are jammed together, even for repulsive energies in excess of 5 kcal/mol. As may be seen in Figure S3, the NCI is consistent with this narrative, even showing a green attractive region which turns blue for very short contact.

3.1.5 | Anion-anion interaction

A good deal of recent work^{51-60,78-80} has demonstrated that, contrary to a popular assumption, a pair of ions of like charge can attract one another under certain circumstances and form a complex that resists dissociation. In most cases, the formation of a stable dimer, lower in energy than the two separate monomers, requires a polarizable environment, as in solution or within a crystal. However, complexation can occur even in the gas phase, with no external environmental factors. In these cases, the complex is usually metastable; that is, the dimer is less stable than the isolated monomers, but its dissociation is hindered by the presence of an energy barrier.

One particular example that was studied here occurs for the pairing of MgCl $_3^-$ with CN $^-$, in which the latter approaches the former along its C $_3$ symmetry axis, forming a Mg $\cdot\cdot$ N noncovalent bond as pictured in Figure 1E. 81 In its isolated state, MgCl $_3^-$ is planar, and undergoes pyramidalization to accommodate the approaching anion. In order to include this important phenomenon, the geometry of the complex was fully optimized for each value of $R(Mg\cdot\cdot N)$, subject only to C $_{3v}$ symmetry. The energetic data in Table 5 shows the metastable character of the minimum that occurs for R=2.06 Å. Its energy is higher than that of separated anions by 25.9 kcal/mol but stretching causes a rise in the energy, as of course does a compression.

The presence of the Mg··N bond is manifested by the various AIM, NBO, and NCI markers in Table 5. The bond critical point density is 0.045 au, and the second-order perturbation energy for charge transfer from the N lone pair to the vacant Mg p-orbital is 32.9 kcal/mol. NCI also signals the presence of this bond, as pictured in Figure S4. It is worth noting that the various markers of the Mg··N bond increase smoothly and monotonically as the bond distance is shortened, in contrast to the energy which undergoes fluctuations, lowest for R=2.06 Å and more repulsive for both shorter and longer distances.

TABLE 5 Behavior of various properties as CN⁻ anion approaches MgCl₃⁻

R(H.·H) (Å)	E _b (kcal/mol)	ho (au)	$ abla^2 ho$ (au)	−V (au)	E(2) (kcal/mol)	sign(λ_2) $ ho$ (au)
3.50	48.20	0.0021	0.0053	0.0008	0.8	-0.0021
3.00	43.63	0.0053	0.0193	0.0030	4.9	-0.0053
2.60	36.18	0.0130	0.0613	0.0101	14.4	-0.0135
2.30	29.10	0.0260	0.1461	0.0275	25.0	-0.0286
2.06	25.92	0.0452	0.2888	0.0635	32.9	-0.0405
1.90	28.93	0.0664	0.4662	0.1138	37.1	-0.0491
1.70	47.55	0.1072	0.8568	0.2301	40.4	-0.0350

FIGURE 4 Systems examined in relation to angular deformation as defined by θ angle

TABLE 6 Behavior of various properties as CIH molecule is rotated within the CIH··NH₄ dimer

θ R	R B	θ R (C)
(A)	(B)	(C) Q H

θ (°)	E _b (kcal/mol)	ho (au)	$ abla^2 ho$ (au)	−V (au)	E(2) (kcal/mol)	$\operatorname{sign}(\lambda_2)\rho$ (au)
0	-8.97	0.0596	0.0461	0.0537	46.4	-0.0499
20	-4.38	0.0437	0.0677	0.0356	26.3	-0.0498
40	1.13	0.0210	0.0713	0.0134	4.5	-0.0226^{a}
60	3.43	0.0140 ^b	0.0533 ^b	0.0092 ^b	0.2	-0.0147^{a}
80	4.68	0.0138 ^b	0.0507 ^b	0.0085 ^b	-	-0.0140^{b}

^aBlend of H··N and Cl··N.

3.2 | Angular dependence

3.2.1 | H-bond

It is widely understood that a H-bond prefers a linear arrangement with the proton situated roughly along the axis between the proton donor and acceptor atoms. The manner in which the various bond strength indicators might support this idea was tested in the context of the CIH...NH₃ complex. As illustrated in Figure 4A, the proton was bent away from the Cl··N axis by an angle θ , with the R(Cl··N) distance fixed at its optimized value of 3.04 Å. As is evident in Table 6, the binding energy of this complex quickly turns from strongly attractive to quite repulsive as θ varies from 0° to 80°. The density of the H.·N bond critical point density declines, echoing this bond weakening, as does the potential energy density V. However, for a distortion angle of 60° and above, the AIM diagram presents a bond path between the N and the Cl atom, although such a bond is doubtful. The density at this critical point is some 0.014 au, and its Laplacian is 0.05 au. After its initial decline, V hovers at around -0.009 au for the putative Cl··N bond path. Unlike AIM, NBO does not suggest a Cl.·N bond, as E(2) for the $N_{lp} \to \sigma^*$ (CIH) transfer drops precipitously as the H-bond is deformed.

^bRefers to bond between Cl and N.

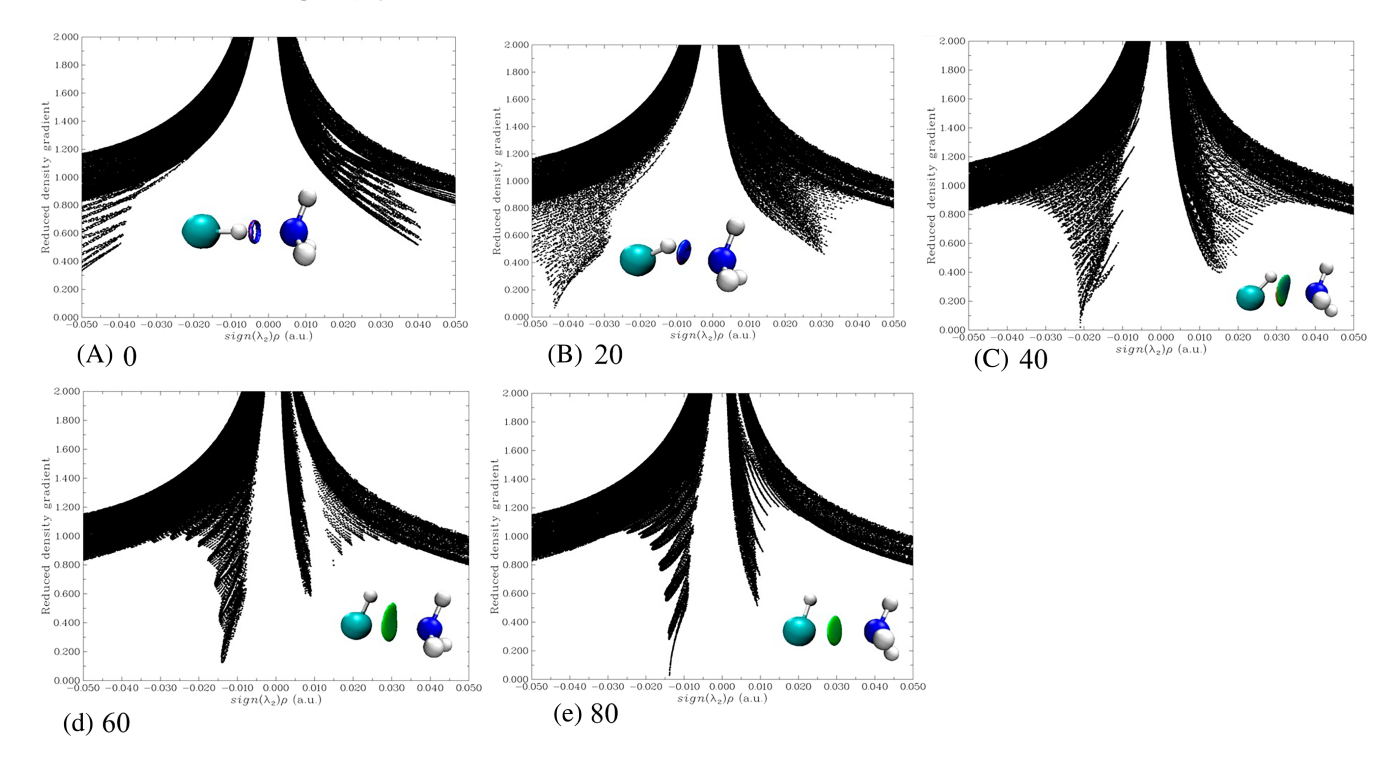


FIGURE 5 NCI diagrams of CIH··NH₃ complex as CIH is rotated for various values of θ (°). Extrema of sign(λ_2) ρ are shown in blue for -0.035 au and red for +0.020 au

<i>θ</i> (°)	E _b (kcal/mol)	ho (au)	$ abla^2 ho$ (au)	−V (au)	E(2) (kcal/mol)	$\operatorname{sign}(\lambda_2) \rho$ (au)
93.8	-3.11	0.0184	0.0555	0.0127	10.5	-0.0201
115	-2.33	0.0180	0.0552	0.0125	9.8	-0.0192
135	-0.37	0.0164	0.0526	0.0116	7.3	-0.0176
155	1.96	0.0139	0.0495	0.0102	4.2	-0.0148
180	3.18	0.0115	0.0500	0.0094	2.3	-0.0118

TABLE 7 Behavior of various properties as electron donor molecule of FBr dimer is rotated

NCI, like AIM, is consistent with the idea of the H-bond mutating into a CI-·N bond as the CIH is rotated. This transformation is visualized in Figure 5. The strong H-bond for $\theta=0^\circ$ is clearly visible as the blue ring along the axis. As the H is lifted from the CI-·N axis, this blue disk moves along with the proton, then weakens to a green color for $\theta=40^\circ$. The extended shape of this green disk in Figure 4c suggests the beginning of a CI-·N bond which is more obvious for 60° . Once the H has been rotated by 80° , the green disk has moved to lie directly along the CI-·N axis, signaling an attractive interaction between these two atoms.

3.2.2 | Halogen bond

Like the H-bond, the halogen bond is also highly directional, perhaps even more so. This aspect of these bonds was examined with the aid of the FBr dimer. As pictured in Figure 4B, the behavior of the halogen bond was monitored as the θ angle was varied from its optimal

value of 93.8° which would place a lone pair of the unit on the right in maximal coincidence with both the σ -hole and $\sigma^*(FBr)$ orbital of the electron acceptor on the left. As θ is increased, the righthand unit rotates so as reduce the overlap between the pertinent orbitals while further destabilizing the system by placing the positive σ -holes of the two monomers in coincidence with one another. This transformation from an attractive to a repulsive interaction is evident from the change in sign of E_b in Table 7 as θ increases, retaining the $R(Br \cdot \cdot Br)$ distance at its optimal 3.13 Å. The Br. Br bond critical point mirrors this bond weakening, as does V. The NBO measure of bond strength likewise drops along with the bond distortion, as does sign $(\lambda_2)\rho$. The density Laplacian is a bit of an outlier in that it remains fairly flat as θ rises. Figure S5 mimics the bond weakening by the slow rightward drift of the lefthand cusp, while the disk between the two Br atoms remains attractive green throughout. In other words, while the various bond indicators do present evidence of a weakening, they all erroneously suggest the bond persists even in the face of a repulsive potential.

TABLE 8 Behavior of various properties as NH₃ is displaced from optimal orientation in complex with H₂CO

<i>θ</i> (°)	E _b (kcal/mol)	ho (au)	$ abla^2 ho$ (au)	−V (au)	E(2) (kcal/mol)	sign(λ_2) ρ (au)
62	0.55	0.0219	0.1251	0.0229	1.3	-0.0233
82	-3.55	0.0130	0.0507	0.0507	3.0	-0.0134
102	-3.97	0.0128	0.0457	0.0457	4.3	-0.0135
122	-3.39	0.0136	0.0516	0.0516	4.6	-0.0144
142	-2.02	0.0148	0.0603	0.0603	3.8	-0.0155

3.2.3 | π -Hole tetrel bond

The rotation of the electron donor away from its optimal orientation is delineated in Figure 4c by the $\theta(\text{OC}\cdot\cdot\text{N})$ angle. For each angle chosen for study, the $R(\text{C}\cdot\cdot\text{N})$ distance was held steady at the optimal 2.808 Å, and the internal geometry of $H_2\text{CO}$ was fixed, but all other parameters were fully optimized. Table 8 details that a deviation in either direction from the optimal angle of 102° raises the energy of the system. This rise is particularly notable for smaller angles that move the N closer to the O with its partial negative charge. A 40° displacement in this direction makes the interaction a repulsive one.

The behavior of the AIM markers is anomalous in some respects. Even though the tetrel bond weakens in either direction of deviation, the BCP density ascends, as does its Laplacian. The potential energy density V behaves in a similar manner with the exception of a substantial drop for $\theta=62^\circ$. With regard to the NBO measure of $N_{lp}\to\pi^*(CO)$ charge transfer, this quantity peaks at 122° , some 20° larger than the optimal angle. NCI data does not offer much information about preferred orientation. In fact, $sign(\lambda_2)_P$ attains its most negative value for $\theta=62^\circ$, where the binding energy is positive. The insets of Figure S6 are rather similar to one another, with a green attractive region between the two subunits, whether the interaction is attractive or repulsive.

4 | DISCUSSION

It is clear from the results presented above that neither AIM, NCI, nor NBO indicators can be taken as indisputable evidence of a noncovalent bond. These measures signal the presence of such a bond even when the two molecules are placed close enough together that their mutual steric repulsion dwarfs any attractive components that might be present. This situation is not limited only to a slightly squeezed interaction, but these indicators continue their upward climb even when this compression continues and the repulsive force is dominant. This finding appears to be a general phenomenon occurring in the H-bond, halogen bond, and the π -hole tetrel bond. The overly close approach of two H atoms, both bonded to C and bearing similar charges, also lends itself to the false impression of a stabilizing interaction where none such is present. The approach of two anions toward one another can lead to a minimum in the potential energy surface, supported by AIM, NBO, and NCI indicators of a noncovalent bond. However, this structure is only metastable, significantly higher in energy than the pair of separated monomers, so it is debatable as

to whether this structure contains a bond in the usual sense. In either case, these measures of bond strength continue to climb even when these two anions are brought in much closer to one another, where the interaction is unarguably repulsive.

It is not only compression of the two molecules when they approach one another too closely where this phenomenon appears, but also in the context of angular deformations. The reorientation of the two molecules within a hydrogen or halogen bond, which disrupts this bond and converts the interaction to a repulsive one, nonetheless contains indicators of the presence of a stabilizing interaction, and the same is true for a π -hole tetrel bond. In one case, the disruption of the H-bond of CIH.·NH₃ by the rotation of the proton donor led to AIM and NCI indications of the formation of a stabilizing interaction between the CI and N atoms even though the total binding energy is quite positive. A similar rotation within the halogen-bonded complex caused only minor modifications of some of these indicators even as the binding energy grew large and positive. It is also notable that the displacement of the electron donor from its optimal position above the C of H_2CO raised the AIM and NCI markers of a π -tetrel bond even as the interaction became repulsive.

One might argue that these findings signify that a bond is indeed present in these cases, but that it is overwhelmed by highly repulsive steric forces. Indeed SAPT breakdown of the interaction energy of the halogen bonded FBr.·NH₃ complex shows that the electrostatic, induction, and dispersion energies are all-attractive and become even more so as the two units are squeezed together, but are opposed by a precipitous rise of the exchange repulsion. A similar pattern emerges for the interaction between two anions. The overall Coulombic interaction is indeed repulsive for the initial approach of the two anions in the MgCl₃⁻ ···NC⁻ system. However, the SAPT electrostatic term becomes negative for their metastable equilibrium geometry, and becomes progressively more attractive for even closer approach. Therefore, since the AIM, NCI, and NBO quantities represent measures of electron density perturbation and charge transfer, it is not surprising that they rise as the two monomers more closely approach one another, even as they pass beyond the minimum total energy where the attractive and repulsive forces are in equilibrium. However, what is usually meant by the presence of a noncovalent bond is that there is an overall net attractive force, where the sum of the attractive components outweighs the repulsive term.

To use the CH··HC interaction as an example, the identification of an AIM bond path between the two H atoms is usually interpreted as a component of the overall attraction between the two molecules involved. However, the findings presented above indicate that no

such attraction necessarily exists, bond path notwithstanding, and that the H··H interactions are likely repulsive. Of course, the particular example chosen of a methane dimer is not representative of all interactions between alkyl groups. It is known that CH··HC interactions can be attractive and a factor in overall molecular structure in certain instances. ^{82–86} The main point is that AIM bond paths are not sufficient evidence of such stabilizing interactions in the general case.

It should be emphasized that the behavior of the noncovalent bond indicators discussed herein do not rule out their usefulness in interpreting the underlying nature of the interactions between molecules. For example, both ρ and V have been found to be fairly accurate measures of the strengths of interactions such as H-bonds, and the NCI index is commonly used to compare bond strengths with one another. In addition, NBO is of great value in estimating the quantitative contribution of charge transfer to a molecular interaction, as well as pinpointing which orbitals are involved. The value of these measures is maximized when the interaction of interest is the only one present, or is the primary one. In these cases, the distance between the two subunits is guided by this noncovalent bond, which results in a balance between its attractive and repulsive components. The problem arises when the intermolecular geometry is determined largely by other forces. For example, one or more noncovalent bonds elsewhere in a complex might draw a halogen atom too close to a N atom of the other subunit, to the point that this particular interatomic interaction becomes repulsive. Yet their proximity to one another might lead to noncovalent bond indices of substantial magnitude, and to the incorrect inference of a halogen bond which contributes to the overall stability of the complex when in fact it tends to destabilize it. Indeed, if drawn in close enough, the large bond markers might even erroneously suggest it is this noncovalent (non)bond which is the driving force in the complexation.

The ability of AIM bond paths to constitute proof of a stabilizing interaction has been questioned in the past from both a practical 36,40 and a formal perspective. 41 Myburgh et al. 42 noted that spurious H··H bond paths can emerge if the H atoms are placed in close proximity. The Jablonski group has pointed to the association of such bond paths with repulsive interactions 43,44,87 as well as other weaknesses in this interpretation. 88,89 Other workers noted these paths might be misleading in other ways 0 and discrepancies between conclusions reached on the basis of AIM as compared to NBO. 35 Dunitz 39 pointed out that one frequently encounters short interatomic distances in crystals, many of which are not indicative of any sort of bonding interaction, but due instead simply to overlapping of atomic electron densities. This idea was buttressed by later work from a crystal perspective. 91

5 | CONCLUSIONS

Based on the results presented here, and in countless previous computational works, NBO, AIM, and NCI indices seem to represent an appropriate and accurate means of assessing the energetic strength of various noncovalent bonds when the two subunits are placed at their equilibrium distances and orientations, and can even help quantify the destabilization as the two monomers are pulled apart. On the other hand, these markers continue to grow even as the system is destabilized by pulling the two subunits in closer than their preferred separation, and the repulsive forces overwhelm any attractive components. Similar observations apply to certain angular deformations which can even lead to spurious indications of a bond between two atoms when none clearly exists. These methods also indicate the presence of an attractive interaction between H atoms in a CH··HC arrangement where no such bond occurs, nor do they correctly reproduce the behavior of the energy as two anions approach one another.

It is thus advised that due caution be applied to indicators of the presence of a bond when there is some question raised from chemical reasoning. For example, when two atoms on different subunits are drawn in close to one another by the presence of other noncovalent bonds, crystal packing, or other physical phenomena, it is possible that these computational protocols might suggest the presence of a bonding interaction when this particular contact is better characterized as repulsive.

ACKNOWLEDGMENTS

This material is based upon work supported by the National Science Foundation under Grant No. 1954310.

CONFLICT OF INTEREST

The author declares no conflict of interest.

DATA AVAILABILITY STATEMENT

The data that support the findings of this study are available from the corresponding author upon reasonable request.

ORCID

Steve Scheiner https://orcid.org/0000-0003-0793-0369

REFERENCES

- [1] G. C. Pimentel, A. L. McClellan, *The Hydrogen Bond*, Freeman, San Francisco **1960**.
- [2] M. D. Joesten, L. J. Schaad, Hydrogen Bonding, Marcel Dekker, New York 1974.
- [3] P. Schuster, G. Zundel, C. Sandorfy, Recent Developments in Theory and Experiments, North-Holland Publishing Co., Amsterdam 1976.
- [4] E. Arunan, G. R. Desiraju, R. A. Klein, J. Sadlej, S. Scheiner, I. Alkorta, D. C. Clary, R. H. Crabtree, J. J. Dannenberg, P. Hobza, H. G. Kjaergaard, A. C. Legon, B. Mennucci, D. J. Nesbitt, *Pure Appl. Chem.* 2011, 83, 1637.
- [5] A. Chand, D. K. Sahoo, A. Rana, S. Jena, H. S. Biswal, Acc. Chem. Res. 2020, 53, 1580.
- [6] A. Karpfen, in Halogen Bonding. Fundamentals and Applications (Eds: P. Metrangolo, G. Resnati), Springer, Berlin 2008, p. 1.
- [7] K. E. Riley, P. Hobza, J. Chem. Theory Comput. 2008, 4, 232.
- [8] C. B. Aakeröy, M. Fasulo, N. Schultheiss, J. Desper, C. Moore, J. Am. Chem. Soc. 2007, 129, 13772.
- [9] T. Clark, M. Hennemann, J. S. Murray, P. Politzer, J. Mol. Model. 2007, 13, 291.
- [10] S. J. Grabowski, Phys. Chem. Chem. Phys. 2013, 15, 7249.

- [11] S. Zahn, R. Frank, E. Hey-Hawkins, B. Kirchner, Chem. Eur. J. 2011, 17, 6034
- [12] A. Bauzá, D. Quiñonero, P. M. Deyà, A. Frontera, CrystEngComm 2013, 15, 3137.
- [13] S. Scheiner, Acc. Chem. Res. 2013, 46, 280.
- [14] H. S. Biswal, A. K. Sahu, B. Galmés, A. Frontera, D. Chopra, ChemBio-Chem 2022, 23, e202100498.
- [15] Q. Li, H. Zhuo, X. Yang, J. Cheng, W. Li, R. E. Loffredo, Chem-PhysChem 2014, 15, 500.
- [16] G. Sanchez-Sanz, C. Trujillo, I. Alkorta, J. Elguero, Phys. Chem. Chem. Phys. 2014, 16, 15900.
- [17] J. E. Del Bene, I. Alkorta, J. Elguero, in Noncovalent Forces (Ed: S. Scheiner), Springer, Dordrecht, Netherlands 2015, p. 191.
- [18] A. Bauza, T. J. Mooibroek, A. Frontera, Chem. Commun. 2015, 51, 1491
- [19] H. S. Biswal, A. Kumar Sahu, A. Frontera, A. Bauzá, J. Chem. Inf. Model. 2021, 61, 3945.
- [20] S. J. Grabowski, Phys. Chem. Chem. Phys. 2017, 19, 29742.
- [21] V. R. Mundlapati, D. K. Sahoo, S. Bhaumik, S. Jena, A. Chandrakar, H. S. Biswal, Angew. Chem. Int. Ed. 2018, 57, 16496.
- [22] M. Solimannejad, V. Ramezani, C. Trujillo, I. Alkorta, G. Sánchez-Sanz, J. Elguero, J. Phys. Chem. A 2012, 116, 5199.
- [23] M. D. las Nieves Piña, S. Burguera, J. Buils, M. Àngel, J. E. M. Crespí, J. Pons, A. Bauzá, A. Frontera, ChemPhysChem 2022, 23, e202200010.
- [24] M. L. Kuznetsov, Molecules 2021, 26, 2083.
- [25] B. Galmés, J. Adrover, G. Terraneo, A. Frontera, G. Resnati, Phys. Chem. Chem. Phys. 2020, 22, 12757.
- [26] M. G. Sarwar, B. Dragisic, L. J. Salsberg, C. Gouliaras, M. S. Taylor, J. Am. Chem. Soc. 2010, 132, 1646.
- [27] N. Kumar, S. Saha, G. N. Sastry, Phys. Chem. Chem. Phys. 2021, 23, 8478.
- [28] M. Rozenberg, RSC Adv. 2014, 4, 26928.
- [29] E. Espinosa, E. Molins, C. Lecomte, Chem. Phys. Lett. 1998, 285, 170.
- [30] E. Espinosa, I. Alkorta, J. Elguero, E. Molins, J. Chem. Phys. 2002, 117, 5529.
- [31] D. F. Mertsalov, R. M. Gomila, V. P. Zaytsev, M. S. Grigoriev, E. V. Nikitina, F. I. Zubkov, A. Frontera, CrystEngComm 2021, 11, 1406.
- [32] D. K. Miller, I. Y. Chernyshov, Y. V. Torubaev, S. V. Rosokha, Phys. Chem. Chem. Phys. 2022, 24, 8251.
- [33] X. Wang, B. Li, H. Wang, Q. Song, Y. Ni, H. Wang, Chem. Phys. Lett. 2022, 791, 139377.
- [34] S. J. Grabowski, Molecules 2020, 25, 4668.
- [35] F. Weinhold, P. V. R. Schleyer, W. C. McKee, J. Comput. Chem. 2014, 35, 1499.
- [36] C. R. Wick, T. Clark, J. Mol. Model. 2018, 24, 142.
- [37] S. Scheiner, Cryst. Growth Des. 2022, 22, 2692.
- [38] S. Scheiner, J. Phys. Chem. A 2022, 126, 1194.
- [39] J. D. Dunitz, IUCrJ 2015, 2, 157.
- [40] Z. A. Keyvani, S. Shahbazian, M. Zahedi, Chem. Eur. J. 2016, 22, 5003.
- [41] S. Shahbazian, Chem. Eur. J. 2018, 24, 5401.
- [42] D. Myburgh, S. von Berg, J. Dillen, J. Comput. Chem. 2018, 39, 2273.
- [43] M. Jablonski, M. Palusiak, Chem. Phys. 2013, 415, 207.
- [44] M. Jablonski, J. Phys. Chem. A 2012, 116, 3753.
- [45] E. C. Escudero-Adán, A. Bauzá, C. Lecomte, A. Frontera, P. Ballester, Phys. Chem. Chem. Phys. 2018, 20, 24192.
- [46] C. F. Matta, J. Hernández-Trujillo, T.-H. Tang, R. F. W. Bader, Chem. Eur. J. 1940, 2003, 9.
- [47] J. Poater, M. Solà, F. M. Bickelhaupt, Chem. Eur. J. 2006, 12, 2889.
- [48] J. Poater, F. M. Bickelhaupt, M. Solà, J. Phys. Chem. A 2007, 111, 5063.
- [49] I. Stylianakis, A. Shalev, S. Scheiner, M. P. Sigalas, I. T. Arkin, N. Glykos, A. Kolocouris, J. Comput. Chem. 2020, 41, 2177.
- [50] A. Singh, D. K. Sahoo, S. K. Sethi, S. Jena, H. S. Biswal, Chem-PhysChem 2017, 18, 3625.

- [51] L. Chen, Q. Feng, C. Wang, S. Yin, Y. Mo, J. Phys. Chem. A 2021, 125, 10428.
- [52] J. M. Holthoff, R. Weiss, S. V. Rosokha, S. M. Huber, Chem. Eur. J. 2021, 27, 16530.
- [53] A. Daolio, A. Pizzi, G. Terraneo, A. Frontera, G. Resnati, Chem-PhysChem 2021, 22, 2281.
- [54] F. Yang, K. A. Behrend, H. Knorke, M. Rohdenburg, A. Charvat, C. Jenne, B. Abel, J. Warneke, Angew. Chem. Int. Ed. 2021, 60, 24910.
- [55] C. Loy, J. M. Holthoff, R. Weiss, S. M. Huber, S. V. Rosokha, Chem. Sci. 2021, 12, 8246.
- [56] A. Daolio, A. Pizzi, G. Terraneo, M. Ursini, A. Frontera, G. Resnati, Angew. Chem. Int. Ed. 2021, 60, 14385.
- [57] L. M. Azofra, J. Elguero, I. Alkorta, Phys. Chem. Chem. Phys. 2020, 22, 11348.
- [58] D. Quiñonero, I. Alkorta, J. Elguero, ChemPhysChem 2020, 21, 1597.
- [59] W. Zierkiewicz, M. Michalczyk, T. Maris, R. Wysokiński, S. Scheiner, Chem. Commun. 2021, 57, 13305.
- [60] M. Michalczyk, W. Zierkiewicz, R. Wysokiński, S. Scheiner, Phys. Chem. Chem. Phys. 2021, 23, 25097.
- [61] M. J. Frisch, G. W. Trucks, H. B. Schlegel, G. E. Scuseria, M. A. Robb, J. R. Cheeseman, G. Scalmani, V. Barone, G. A. Petersson, H. Nakatsuji, X. Li, M. Caricato, A. V. Marenich, J. Bloino, B. G. Janesko, R. Gomperts, B. Mennucci, H. P. Hratchian, J. V. Ortiz, A. F. Izmaylov, J. L. Sonnenberg, F. D. Williams, F. Lipparini, F. Egidi, J. Goings, B. Peng, A. Petrone, T. Henderson, D. Ranasinghe, V. G. Zakrzewski, J. Gao, N. Rega, G. Zheng, W. Liang, M. Hada, M. Ehara, K. Toyota, R. Fukuda, J. Hasegawa, M. Ishida, T. Nakajima, Y. Honda, O. Kitao, H. Nakai, T. Vreven, K. Throssell, J. A. Montgomery Jr., J. E. Peralta, F. Ogliaro, M. J. Bearpark, J. J. Heyd, E. N. Brothers, K. N. Kudin, V. N. Staroverov, T. A. Keith, R. Kobayashi, J. Normand, K. Raghavachari, A. P. Rendell, J. C. Burant, S. S. Iyengar, J. Tomasi, M. Cossi, J. M. Millam, M. Klene, C. Adamo, R. Cammi, J. W. Ochterski, R. L. Martin, K. Morokuma, O. Farkas, J. B. Foresman, D. J. Fox, Gaussian 16 Rev. C.01, Gaussian, Inc Wallingford, CT 2016.
- [62] Y. Zhao, D. G. Truhlar, Theor. Chem. Accounts 2008, 120, 215.
- [63] R. A. Kendall, T. H. D. Jr, R. J. Harrison, J. Chem. Phys. 1992, 96, 6796.
- [64] F. De Vleeschouwer, F. De Proft, Ö. Ergün, W. Herrebout, P. Geerlings, Molecules 2021, 26, 6767.
- [65] P. R. Varadwaj, A. Varadwaj, H. M. Marques, K. Yamashita, Int. J. Mol. Sci. 2022, 23, 1263.
- [66] L. de Azevedo Santos, T. C. Ramalho, T. A. Hamlin, F. M. Bickelhaupt, J. Comput. Chem. 2021, 42, 688.
- [67] Y. Chen, F. Wang, ACS Omega 2020, 5, 30210.
- [68] A. Li, H. S. Muddana, M. K. Gilson, J. Chem. Theory Comput. 2014, 10, 1563.
- [69] N. Mardirossian, M. Head-Gordon, J. Chem. Theory Comput. 2013, 9, 4453.
- [70] T. A. Keith, AIMAII, Overland Park, KS, TK Gristmill Software 2013.
- [71] T. Lu, F. Chen, J. Comput. Chem. 2012, 33, 580.
- [72] W. Humphrey, A. Dalke, K. Schulten, J. Mol. Graph. 1996, 14, 33.
- [73] A. E. Reed, L. A. Curtiss, F. Weinhold, J. Chem. Phys. 1985, 83, 735.
- [74] A. E. Reed, L. A. Curtiss, F. Weinhold, Chem. Rev. 1988, 88, 899.
- [75] B. Jeziorski, R. Moszynski, K. Szalewicz, Chem. Rev. 1994, 94, 1887.
- [76] K. Szalewicz, B. Jeziorski, in Molecular Interactions. From Van der Waals to Strongly Bound Complexes (Ed: S. Scheiner), Wiley, New York 1997, p. 3.
- [77] H.-J. Werner, P. J. Knowles, F. R. Manby, M. Schütz, P. Celani, G. Knizia, T. Korona, R. Lindh, A. Mitrushenkov, G. Rauhut, T. B. Adler, R. D. Amos, A. Bernhardsson, A. Berning, D. L. Cooper, M. J. O. Deegan, A. J. Dobbyn, F. Eckert, E. Goll, C. Hampel, A. Hesselmann, G. Hetzer, T. Hrenar, G. Jansen, C. Köppl, Y. Liu, A. W. Lloyd, R. A. Mata, A. J. May, S. J. McNicholas, W. Meyer, M. E. Mura, A. Nicklaß, P. Palmieri, K. Pflüger, R. Pitzer, M. Reiher, T. Shiozaki, H. Stoll, A. J. Stone, R. Tarroni, T. Thorsteinsson, M. Wang, M. Welborn, MOLPRO, 2010, 3.

- [78] D. Fan, L. Chen, C. Wang, S. Yin, Y. Mo, J. Chem. Phys. 2021, 155, 234302.
- [79] Y. Li, L. Meng, Y. Zeng, ChemPlusChem 2021, 86, 232.
- [80] L. M. Azofra, J. Elguero, I. Alkorta, J. Phys. Chem. A 2020, 124, 2207.
- [81] W. Zierkiewicz, R. Wysokiński, M. Michalczyk, S. Scheiner, Chem-PhysChem 2020, 21, 870.
- [82] K. L. Mears, P. P. Power, Acc. Chem. Res. 2022, 55, 1337.
- [83] C.-Y. Lin, J.-D. Guo, J. C. Fettinger, S. Nagase, F. Grandjean, G. J. Long, N. F. Chilton, P. P. Power, *Inorg. Chem.* 2013, 52, 13584.
- [84] H. Schwertfeger, A. A. Fokin, P. R. Schreiner, Angew. Chem. Int. Ed. 2008, 47, 1022.
- [85] J.-D. Guo, D. J. Liptrot, S. Nagase, P. P. Power, Chem. Sci. 2015, 6, 6235.
- [86] J.-D. Guo, S. Nagase, P. P. Power, Organometallics 2028, 2015, 34.
- [87] M. Jabłoński, Chem. Phys. Lett. 2020, 759, 137946.

- [88] M. Jabłoński, J. Comput. Chem. 2018, 39, 2183.
- [89] M. Jabłoński, ChemistryOpen 2019, 8, 497.
- [90] I. Alkorta, G. Sanchez-Sanz, J. Elguero, J. Phys. Chem. A 2014, 118, 1527.
- [91] R. Taylor, CrystEngComm 2020, 22, 7145.

SUPPORTING INFORMATION

Additional supporting information can be found online in the Supporting Information section at the end of this article.

How to cite this article: S. Scheiner, *J. Comput. Chem.* **2022**, 43(26), 1814. https://doi.org/10.1002/jcc.26983